Adaptive time-stepping in diffeomorphic image registration with bounded inverse consistency error

Akshay Pai[1], Stefan Klein[3], Stefan Sommer[1], Lauge Sørensen[1,2], Sune Darkner[1], Jon Sporring[1] and Mads Nielsen[1,2]

[1] DIKU, University of Copenhagen, Copenhagen,
[2] Biomediq A/S, Copenhagen
[3] Biomedical Imaging Group Rotterdam, Depts. of Medical Informatics & Radiology, Erasmus MC, Rotterdam, Netherlands

Abstract. In a continuous setting, diffeomorphisms generated by stationary velocity fields (SVF) are invertible transformations with differentiable inverses. However, due to the numerical integration of the velocity field, inverse consistency is not achieved in practice. In SVF based image registration, inverse consistency is therefore often enforced through a penalty term. Existing penalty terms penalize the inverse consistency error generated by the composition of the forward and backward transformations. However, in such terms, a higher consistency requirement pushes the transformation towards linearity due to the discretization involved and fixed number of integration time-steps. In this paper, we propose a method to both penalize inverse consistency error and to adaptively set the number of integration time-steps required, so that the predicted maximum inverse consistency error is bounded, taking into account discretization errors. This formulation allows more flexibility in the transformation model to realize complex deformations while still achieving the desired level of inverse consistency. Using synthetic examples, we show that the measured inverse consistency and the predicted inverse consistency match. Also, the proposed method is able to achieve more accurate image registration. On the MGH10 dataset, the Jaccard index of the proposed method on inter-subject registration reaches the same level as the registration scheme using a fixed-time step and the conventional penalty term while using a lower number of integration time-steps, thus saving on the computational time.

1 Introduction

Image registration plays a very important role in the field of medical research and clinical applications. It has found utilities in both the longitudinal and cross-sectional characterization of human anatomy. It is particularly useful because it provides localized transformations that can be used to study deformation at an organ level. For instance, image registration in the form of tensor-based morphometry is used to measure atrophy in various brain regions which is then

used to quantify diseases such as the Alzheimer's disease. However, to effectively use transformations from an image registration, they need to be free of any bias. One common bias that has been found to have severe implications on bio-marker quantification like longitudinal atrophy estimation, is the inverse consistency error in transformations [1].

Ideally in image registration, the transformation between two images is expected to be invariant to the order of the choice of source and target. In practice however, such a transformation is not possible due to several reasons such as discrete image information, finite degrees of freedom, and discretization errors due to numerical integration of flow fields. Therefore, inverse consistency is often enforced as a penalty term. The existing inverse consistent methods, particularly pertaining to diffeomorphic approaches, either look at the forward and backward transformations simultaneously [2] or the velocity field by making an assumption that the forward and backward velocity fields are exact negatives of each other [3].

In a continuous setting, the path generated by a velocity field can be exactly retraced. However, in a discrete setting, the path is approximated using a set of piecewise linear steps. Most often retracing these steps will yield an inverse inconsistent transformation. The fewer the time-steps, the higher is the inverse consistency. Also, the higher the curvature of the path, the more steps are required to be close to being inverse consistent. Therefore, if one needs control over the inverse consistency error, the effect of the discretization error needs to be accounted for.

In this paper, we propose a method to both penalize and account for discretization errors. Instead of pushing the inverse consistency error to zero which tends the transformation to linearity, we propose to bound the error by adjusting the number of integration time-steps used to integrate the stationary velocity field (SVF). This lends flexibility in the transformation model to reach more complex deformations while still being reasonably inverse consistent. The main contributions of the paper are as follows,

- We propose to penalize the inverse consistency error based only on the velocity fields. This is achieved using the Baker-Campbell-Hausdorff (BCH) [4] expansion to formulate the theoretical inverse consistency in terms of the velocity field.
- We propose to adjust the required number of integration time-steps prior to each optimization iteration by predicting and thereby bounding the inverse consistency error based on the properties of the velocity field.

Note that through out the paper, we use two sets of parameterizations of the velocity field - one for the forward transformation and one for the backward.

2 Background and Outline

The most commonly used inverse consistency term follows a similar framework as proposed by *Christensen et al* [2] with variations. The method in essence involves

jointly estimating the forward and backward transformations while minimizing the inverse consistency error. While the earlier approach [2] involved estimating both the transformations and its inverses, the current approaches [5], just maintain two transformations and through the penalty term, push them to be inverse consistent. In a different approach [6], the proposed model incorporated stochastic errors in the inverse consistent constraints as a post-processing step. Further in [7], the gradient descent updates of the forward and backward transformations were symmetrized by estimating a linear Taylor series expansion of the inverse consistency condition. Another class of inverse consistent registration scheme warps the image to a mid point [8], median [9] or to a mean shape [10]. The popular logDemons approach on the other hand assumes the forward velocity field is the negative of the backward velocity field to maintain inverse consistency [3]. In the method we propose to adjust the number of integration time steps during the registration optimization to bound the inverse consistency error. And, in order to ensure the number of time-steps is in a reasonable range, we also add a penalty term.

We begin with introducing the stationary velocity field based image registration method followed by presenting the Wendland kernel bundle framework used as a transformation model. We will then discuss our contribution where the inverse consistency term and the predictive inverse consistency term are proposed. We will then present some experiments on synthetic examples and also on the publicly available MGH10 dataset.

3 Registration

Given a floating image S_1 and a reference image S_2 with a spatial domain $\Omega \in \mathbb{R}^d$, image registration involves finding a transformation $\varphi : \Omega \to \Omega$ that aligns these images. We maintain two warps φ_f, φ_b: one for a forward transformation and the second for backward. The transformation is a result of minimizing the dissimilarity between the images under certain constraints encoded in the regularization term. A general cost function is of the form:

$$\begin{aligned} E(\varphi_f, \varphi_b) = \arg\min_{\varphi_f, \varphi_b} & E_D(S_1(\varphi_f), S_2) + E_D(S_2(\varphi_b), S_1) + \lambda_R E_{R_f}(\varphi_f, \varphi_b) \\ & + \lambda_{\text{ICC}} E_{\text{ICC}_f}(\varphi_f, \varphi_b) + \lambda_R E_{R_b}(\varphi_b, \varphi_f) \\ & + \lambda_{\text{ICC}} E_{\text{ICC}_b}(\varphi_b, \varphi_f). \end{aligned} \tag{1}$$

where $\lambda_R, \lambda_{\text{ICC}}$ are the user-specified constants, E_D is a dissimilarity measure that allows comparison of the floating image to the reference image, E_R is a regularization term that encodes desired properties of φ, and E_{ICC} is an additional penalty term to enforce inverse consistency which is the focus of this paper. Normalized mutual information (NMI) [11] is used as the similarity measure in this paper.

Let Diff(Ω) be the space containing the diffeomorphic transformation $\varphi : \Omega \to \Omega$, $\phi : \Omega \times \mathbb{R} \to \Omega$ and finally, $\mathbf{v} : \Omega \to \mathbb{R}^d$ be the velocity field belonging

to the tangent space of Diff(Ω) at identity Id. In SVFs, the governing differential equation can be written as:

$$\frac{\partial \phi(\mathbf{x}, t)}{\partial t} = \mathbf{v}(\phi(\mathbf{x}, t)), \quad \varphi = \phi(\mathbf{x}, 1) = \mathrm{Exp}(\mathbf{v}), \tag{2}$$

ϕ, φ represent both forward and backward transformations. The final transformation is then defined as the Lie group exponential map $\mathrm{Exp}(\mathbf{v})$. This Lie group exponential is realized as an Euler integration.

3.1 Wendland kernels

Instead of the usual approach of first choosing a operator and then constructing a reproducing kernel Hilbert space (RKHS), the reproducing kernels with an associated RKHS was directly chosen [12, 13]. One example of such a reproducing kernel is the class of Wendland basis functions [14]. They are particularly interesting because of their finite support and smoothness properties similar to popularly used B-spline. In addition, they are norm-minimizing.

Wendland kernels are positive definite functions with positive Fourier transforms. They are minimal degree polynomials on $[0, 1]$ and yield C^{2k} (k is the desired degree of smoothness) smooth radial basis functions on $\mathbb{R}^d$. We choose the Wendland kernels $\psi(r) = (1 - r)_+$ and $\psi(r) = (1 - r)_+^4(4r + 1)$ where $(\cdot)_+$ denotes semi-positive definiteness. The velocity field defined in (2) may now be parameterized using Wendland kernels as follows,

$$\mathbf{v}(\mathbf{x}) = \sum_i^N \psi(r(\mathbf{x}_i, \mathbf{x}))\mathbf{p}_i. \tag{3}$$

Note that $r(\mathbf{x}, \mathbf{y}) = \frac{||\mathbf{x}-\mathbf{y}||_2}{a}$, where a is a scaling parameter, $\mathbf{p}_i \in \mathbb{R}^d$ is the coefficient attached with every kernel center $\mathbf{x}_i$, and N is the number of kernels having an influence on $\mathbf{x}$. Due to the reproducing property of the kernel parameterizing the velocity fields, the regularization term E_R is chosen to be the Hilbert norm on the velocity field given by $||\mathbf{v}||_V^2 = \sum_{i,j} \mathbf{p}_i^T \psi(r(\mathbf{x}_i, \mathbf{x}_j))\mathbf{p}_j$.

3.2 Kernel bundle framework

The reasoning behind the need for a multi-scale representation of a deformation has been well discussed in a previous work [15]. In short, the velocity fields are linear sums of individual kernels at L levels. It is represented as,

$$\mathbf{v}(\mathbf{x}) = \sum_{m=1}^{L} \mathbf{v}_m(\mathbf{x}) = \sum_{m=1}^{L} \sum_i^{N_m} \psi_m(r(\mathbf{x}_i^m, \mathbf{x}))\mathbf{p}_i^m. \tag{4}$$

The expression of the optimization to (1) in a kernel bundle framework can be written as,

$$\begin{cases} \arg\min_{\mathbf{v}_{f_1},\mathbf{v}_{b_1}} E(\mathrm{Exp}(\mathbf{v}_{f_1}),\mathrm{Exp}(\mathbf{v}_{b_1})), \\ \arg\min_{\mathbf{v}_{f_2},\mathbf{v}_{b_2}} E(\mathrm{Exp}(\mathbf{v}_{f_1}+\mathbf{v}_{f_2}),\mathrm{Exp}(\mathbf{v}_{b_1}+\mathbf{v}_{b_2})), \\ \vdots \\ \arg\min_{\mathbf{v}_{f_L},\mathbf{v}_{b_L}} E(\mathrm{Exp}(\sum_{m=1}^{L}\mathbf{v}_{f_m}),\mathrm{Exp}(\sum_{m=1}^{L}\mathbf{v}_{b_m})) \end{cases}$$

We sequentially optimize for each space of the velocity fields. The kernels at each level can be of any support. For instance, one can have infinitely supported Gaussian kernels in a coarser registration scale and have compactly supported kernels handle finer resolutions in the registration.

4 Inverse consistency

Usually, inverse consistency is addressed as a penalization of the offset generated by a composition of the forward and backward transformations. If this offset is pushed towards zero while having a fixed number of time-steps, the transformations tend towards linearity. In order to achieve larger deformations in finite steps, one needs to allow some degree of inverse inconsistency due to the discrete nature of the image registration problem. While the existing methods penalize the error, in this paper we propose to both penalize the error and also adjust the number of integration time-steps such that the inverse consistency error is bounded. We will, through the relationship between Lie brackets and inverse consistency, show that the proposed scheme allows for some inverse consistency error in a symmetric fashion.

In the following section, we will address a number of inverse consistency terms. For reading ease, we define the abbreviations early and as follows: I_t is the theoretical inverse consistency, I_p is the commonly used inverse consistency term, $I_p^{\frac{1}{n}}$ is the inverse consistency error for the first composition of the Euler's integration of the velocity field and I_{pd} is the predicted inverse consistency term. We will use the subscripts f, b for forward and backward registration. In addition, the formulation of the backward inverse consistency error will follow the forward unless stated otherwise.

Theoretically, the forward inverse consistency term I_{t_f}, can be expressed as a composition of the forward and backward exponentials,

$$I_{t_f} = \mathrm{Exp}(\mathbf{v}_b)\mathrm{Exp}(\mathbf{v}_f) - \mathbf{x}$$

where $\mathbf{v}_f, \mathbf{v}_b$ are the forward and backward velocity fields respectively. The BCH formula is used to efficiently express this composition in terms of the velocity fields as follows,

$$\begin{aligned} I_{t_f} &= \mathrm{Exp}(\mathbf{v}_f + \mathbf{v}_b + \frac{1}{2}[\mathbf{v}_f, \mathbf{v}_b]) - \mathbf{x}, \\ &= \mathbf{v}_f + \mathbf{v}_b + \frac{1}{2}[\mathbf{v}_f, \mathbf{v}_b] + \mathcal{O}(||\mathbf{v}_f + \mathbf{v}_b + \frac{1}{2}[\mathbf{v}_f, \mathbf{v}_b]||^2). \end{aligned} \tag{5}$$

where $[,]$ is the Lie bracket or the commutator that quantifies the amount of change of $\mathbf{v}_b$ in the direction of $\mathbf{v}_f$. It is expressed as,

$$[\mathbf{v}_f, \mathbf{v}_b] = \nabla \mathbf{v}_b \ \mathbf{v}_f - \nabla \mathbf{v}_f \ \mathbf{v}_b$$

The second line in (5) follows from a linear approximation of the exponential. The commonly used inverse consistency term may be defined as,

$$I_{p_f} = \phi_b(\phi_f(\mathbf{x})) - \mathbf{x}. \tag{6}$$

where ϕ_b and ϕ_f are the results of numerical integration of $\mathbf{v}_b$ and $\mathbf{v}_f$, respectively. This term may also be approximated in terms of the velocity field similar to I_{t_f}. It was shown that the final inverse consistency can be expressed in terms of the step-wise inverse consistency error [5] as follows; assuming n time-steps, we get,

$$\begin{aligned} I_{p_f} &\approx n(I_{p_f}^{\frac{1}{n}}), && (7)\\ &= n(\phi_b^{\frac{1}{n}}(\phi_f^{\frac{1}{n}}(\mathbf{x})) - \mathbf{x}), && (8)\\ &= n(\mathbf{x} + \frac{1}{n}\mathbf{v}_f(\mathbf{x}) + \frac{1}{n}\mathbf{v}_b(\mathbf{x} + \frac{1}{n}\mathbf{v}_f(\mathbf{x})) - \mathbf{x}), && (9)\\ &= \mathbf{v}_f(\mathbf{x}) + \mathbf{v}_b(\mathbf{x}) + \frac{1}{n}\nabla \mathbf{v}_b \ \mathbf{v}_f(\mathbf{x}) + \mathcal{O}(||\frac{1}{n}\mathbf{v}_f||^2). && (10) \end{aligned}$$

Note that (9) was obtained using the Taylor expansion of $\mathbf{v}_b(\mathbf{x} + \frac{1}{n}\mathbf{v}_f(\mathbf{x}))$.

In theory, I_{t_f} and I_{p_f} are equivalent as $n \to \infty$, however in practice they are not since n is finite. This implies that the inverse consistency error term we expect to minimize I_{t_f}/I_{t_b} is different than the inverse consistency error we practically minimize I_{p_f}/I_{p_b}.

In this work, we will propose a new way of handling inverse consistency. What we propose is to use the I_{p_f} for penalization and use a prediction term I_{pd} to adjust the number of integration time-steps such that the inverse consistency is bounded.

Given that we maintain two warps, the predicted inverse consistency error term may be derived as follows,

$$I_{pd} = n(\frac{1}{2}(\phi_b^{\frac{1}{n}}(\phi_f^{\frac{1}{n}}(\mathbf{x})) - \mathbf{x} + \phi_f^{\frac{1}{n}}(\phi_b^{\frac{1}{n}}(\mathbf{x})) - \mathbf{x})) \tag{11}$$

Using (9), we get,

$$\begin{aligned} I_{pd} &= \mathbf{v}_f(\mathbf{x}) + \mathbf{v}_b(\mathbf{x}) + \frac{1}{2n}\nabla \mathbf{v}_b(\mathbf{x}) \ \mathbf{v}_f(\mathbf{x}) + \frac{1}{2n}\nabla \mathbf{v}_f(\mathbf{x}) \ \mathbf{v}_b(\mathbf{x}), && (12)\\ &= \mathbf{v}_f + \mathbf{v}_b + \frac{1}{2n}\{\mathbf{v}_f, \mathbf{v}_b\}. && (13) \end{aligned}$$

We use $\{\}$ since it resembles an anti-commutator. It is sometimes used to construct a Jordan algebra, but that is not our purpose. Since $E_{ICC_f} = ||I_{t_f}||^2$ will be penalized during registration, $\mathbf{v}_f + \mathbf{v}_b$ will already be pushed towards zero.

It is thus fair to discard that term in (13) for prediction purposes. We can then derive the following formula to estimate the number of time steps required to achieve a user-specified inverse consistency I_{max} as:

$$n = \frac{\max_{\mathbf{x}} ||\{\mathbf{v}_f, \mathbf{v}_b\}||}{2I_{max}}. \tag{14}$$

n will therefore give us the number of integration time-steps required to achieve a maximum inverse consistency of I_{max}.

In summary, the proposed method involves using (5) as a penalty term and (14) to predict the number integration time-steps required at each iteration of the registration optimization but setting a user-defined value, I_{max} .

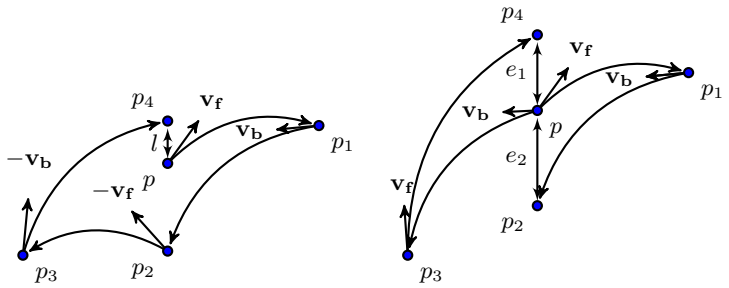

Fig. 1: a) Representation of the Lie Bracket; $l = [\mathbf{v}_f, \mathbf{v}_b]$; b) Representation of $I^{\frac{1}{n}}_{p_f}$ and $I^{\frac{1}{n}}_{p_b}$; $e_1 = I^{\frac{1}{n}}_{p_f}$, $e_2 = I^{\frac{1}{n}}_{p_b}$

The geometric interpretation of a Lie bracket may be seen in Figure 1a. What it represents is that, there is no difference in starting at one point p, traveling a time t over the flow of $\mathbf{v}_f$ and then a time t over the flow of $\mathbf{v}_b$, or, instead, traveling first t over the flow of $\mathbf{v}_b$ and then over the flow of $\mathbf{v}_f$. This is similar to looking at the difference in the step-wise inverse consistency term ($I^{\frac{1}{n}}_{p}$) shown in Figure 1b. We can see that, the Lie Bracket and inverse consistency errors are related since both capture the second order information of the deformation. The formal relation can be shown as follows,

$$I^{\frac{1}{n}}_{p_f} = \frac{1}{n}\mathbf{v}_f(\mathbf{x}) + \frac{1}{n}(\mathbf{v}_b(\mathbf{x}) + \frac{1}{n}\nabla\mathbf{v}_b\mathbf{v}_f(\mathbf{x})). \tag{15}$$

Similarly,

$$\begin{aligned} I^{\frac{1}{n}}_{p_b} &= \phi_f^{\frac{1}{n}}(\phi_b^{\frac{1}{n}}) - \mathbf{x}, \\ &= \frac{1}{n}\mathbf{v}_b(\mathbf{x}) + \frac{1}{n}(\mathbf{v}_f(\mathbf{x}) + \frac{1}{n}\nabla\mathbf{v}_f\mathbf{v}_b(\mathbf{x})),. \end{aligned} \tag{16}$$

Now subtracting (15) and (16):

$$I_{p_f}^{\frac{1}{n}} - I_{p_b}^{\frac{1}{n}} = \frac{1}{n^2}(\nabla \mathbf{v}_b \mathbf{v}_f(\mathbf{x}) - \nabla \mathbf{v}_f \mathbf{v}_b(\mathbf{x})) = \frac{1}{n^2}[\mathbf{v}_f, \mathbf{v}_b]. \tag{17}$$

Using this equivalence, we can redefine our penalty term E_{ICC} as follows:

$$\begin{aligned} E_{ICC_f} &= ||\mathbf{v}_f + \mathbf{v}_b + \frac{1}{2}[\mathbf{v}_f, \mathbf{v}_b]||^2, \\ &= ||\mathbf{v}_f + \mathbf{v}_b + \frac{n^2}{2}(I_{p_f}^{\frac{1}{n}} - I_{p_b}^{\frac{1}{n}})||^2. \end{aligned} \tag{18}$$

and E_{ICC_b} follows the same formulation. Note that the representation of (18) in terms of step-wise inverse consistency error is particularly useful because the gradient of (18) with respect to the transformation parameters yields the terms $\nabla \mathbf{v}_f$ and $\nabla \mathbf{v}_b$ which are required to compute the number of time-steps in (14).

5 Experiments and Results

In this section, we will conduct three experiments to evaluate the performance of the proposed method against the fixed-time step with the conventional inverse consistency regularization method. For evaluation purposes, we will use the following conventional definition of inverse consistency error term, i.e.,

$$\text{ICC} = \frac{1}{k}\sum_{i=1}^{k}\frac{1}{2}(||\varphi_b(\varphi_f(\mathbf{x}_i)) - \mathbf{x}_i||^2 + ||\varphi_f(\varphi_b(\mathbf{x}_i)) - \mathbf{x}_i||^2). \tag{19}$$

where φ_b, φ_f are the backward and forward transformations obtained from integrating the velocity fields $\mathbf{v}_b$ and $\mathbf{v}_f$ respectively and k is the number of voxels.

5.1 Prediction test

In the first of the synthetic experiments, we will compare the predicted inverse consistency error (I_{pd}, (13)) by the proposed method and the measured inverse consistency error (ICC, (19)). We perform this test since (13) is a key to computing the number of integration time-steps. We pick a random scan from the

Mag of CC	I_{pd}(std)	ICC(std)	Max I_{pd}	Max ICC
0.25	0.55 (0.34)	0.53 (0.46)	1.89	2.35
1.0	0.55 (0.43)	0.58 (0.60)	3.68	4.86
2.5	0.63 (0.43)	0.59 (0.67)	2.45	4.79

Table 1: Synthetic example results; Mag of CC: Std of Gaussian used to control the magnitude of the control point coefficient (CC); Units in mm

MGH10 dataset and deform it using a B-spline (control point spacing of 5 mm) whose control coefficients are chosen randomly with a monotonic increase in magnitude. The original images and the deformed images are registered using the Wendland kernel bundle framework together with the common inverse consistency error term (19) and a fixed time-step of 16. Once the optimum velocity fields are estimated, the predicted inverse consistency error (I_{pd}, (13)) is computed. This is compared to the measured inverse consistency error using (19). As Table 1 illustrates, the mean and standard deviation of the inverse consistency error predicted by the proposed method (13) matches that of the measured inverse consistency error (19) indicating that (14) is a fair formulation for estimating the required number of integration time-steps.

5.2 Registration on synthetic example

To test the registration proposed in this paper, we generated synthetic data where the ground truth deformation is known. The synthetic data was generated by deforming the faces of the cube (50^3 mm^3 placed in a 256^3 mm^3 image) using a Gaussian of standard deviation 0.07 (of the cube side length). The deformed and undeformed cubes were registered using the proposed adaptive time-stepping scheme and a conventional scheme with an inverse consistency error penalty as (19) and a fixed number of time-steps of 16 . For both the schemes, the regularization constant was set to 0.1 and two levels of the kernel bundle were used. The first level was parameterized with a kernel of support 4 and the next by a kernel of support 2. I_{max} was set to 1. We set $\lambda_R = 0.3$ and $\lambda_{ICC} = 0.01$. Figure 2 illustrates the source and target images. Following this, the accuracy of the overlap is assessed using the Jaccard index which is given by,

$$\mathrm{JI} = \frac{|S(\phi) \cap T|}{|S(\phi) \cup T|}. \tag{20}$$

where S is the source segmentation, ϕ is the transformation and T is the target segmentation. In addition to this, we measure ICC errors for both the methods using (19). In Table 2, we see that the adaptive scheme showed a better mean overlap (forward and backward) and a very similar inverse consistency error when compared to the fixed-time stepping scheme. However, in the first level of registration the adaptive scheme used only a maximum of 8 time-steps and in the second level it used a maximum of 12 time-steps.

Method	JI	ICC(std)	Max ICC	Max. time steps
Adaptive	0.96	0.01 (0.14)	0.90	8,12
Fixed	0.89	0.01 (0.06)	2.30	16

Table 2: Adaptive scheme versus fixed time-step scheme. Max. time steps: Maximum number of time-steps on level 1 and 2 of the kernel bundle framework.

Fig. 2: Target cube, deformed target cube

5.3 Application on MGH10

We perform an evaluation on the MGH10 dataset[4]. Here the ability to match a set of manually segmented regions of interest via pair-wise registration is evaluated. Each scan is initially reformatted to isotropic voxels (voxel size 1 mm^3 and dimensions of 256^3. The pair-wise images are linearly aligned using 9 DOF. Both the images were mapped to the mid-point of the affine space using the square root of the affine transformation. After the linear alignment, images are non-linearly aligned using the presented registration scheme. Once the registrations are performed, the manual labeled segmentation from the floating image are warped to the reference image using a nearest neighbor interpolation. One

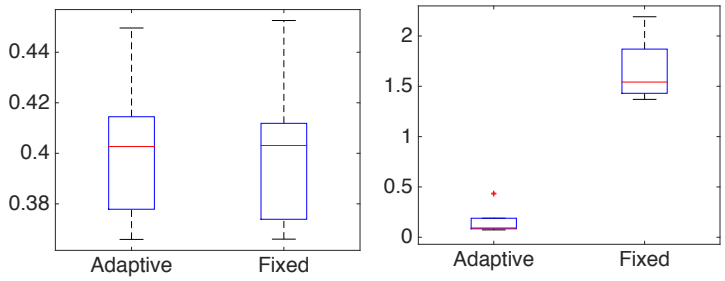

Fig. 3: Box plot of the jaccard index and mean inverse consistency error.

subject is randomly chosen and the other subjects are registered to it. Three levels are used in the kernel bundle. Each level is made of kernels of support 8, 4 and 2 respectively. NMI was used as a similarity measure with 64 bins for the histogram. Images were smoothed with a Gaussian of 0.2 mm. The number of time-steps for the fixed time-step registration scheme was set to 16. The desired maximum inverse consistency error (I_{max}) was set to 1 voxel. We set $\lambda_R = 0.3$ and $\lambda_{ICC} = 0.1$. The comparison is made based in Jaccard Index (20) and ICC error (19). Table 3 indicates that both the methods achieve similar overlaps and inverse consistency errors. However, the adaptive time-stepping scheme

[4] www.mindboggle.info

took fewer number of time-steps for integration. Figure 3 illustrates the overlaps based on both the registration schemes and the mean inverse consistency error.

Method	JI	ICC(std)	Max ICC	Max. time steps
Adaptive	0.39	0.16 (0.21)	1.86	3,6,12
Fixed	0.38	1.65 (1.55)	6.78	16

Table 3: Adaptive scheme versus fixed time-step scheme on MGH10 dataset; Max: mean maximum error.

6 Discussion

In this paper, we presented a way of adjusting the time-steps required to integrate a velocity field such that the maximum inverse consistency error is bounded. We proposed a way to adaptively estimate the number of time-steps based on only the velocity field i.e., without having to realize the entire deformation. We used two terms to handle inverse consistency: one for penalization purposes and the other for time-step prediction. Through the first synthetic experiment we showed that the proposed prediction term produced good estimates of the actual inverse consistency error. The second of the synthetic experiments showed that a higher degree of match and a similar inverse consistency can be achieved using the adaptive time-stepping scheme when compared to the fixed-time step version of registration. On the MGH10 dataset, we showed that the proposed registration scheme reaches the same accuracy as the fixed time-step registration scheme with fewer number of time-steps and a similar inverse consistency.

In a recent version of logDemons [3], the zeroth order of BCH was used to compose two velocity fields. However, in this work since we use $\nabla \mathbf{v}_f \mathbf{v}_b$ and $\nabla \mathbf{v}_b \mathbf{v}_f$ to set the number of time-steps, it makes sense to also take them into account in the penalty term. By using the 1^{st} order BCH term, we keep $\mathbf{v}_f$ more close to $-\mathbf{v}_b$ in regions where $\nabla \mathbf{v}_f \mathbf{v}_b$ and/or $\nabla \mathbf{v}_b \mathbf{v}_f$ are large. In that way we limit the magnitude of $\{\mathbf{v}_f, \mathbf{v}_b\}$.

Two other ways of maintaining inverse consistency are: a) To use a higher order integration scheme. Since higher order integration schemes can be computationally expensive, we restricted our analyses to a forward Euler's scheme. b) By solving for the inverse transformation subject to the inverse consistent condition. This can be computationally expensive since it involves solving a high-dimensional linear system of equations and the transformations need to be estimated sequentially.

The proposed method also saves on computational time since it only takes a relevant number of steps based on the desired inverse consistency level and the properties of the velocity field. This implies, the closer the transformation is to being represented as a small deformation, the lower number of time-steps

are taken. That is, a low $\nabla \mathbf{v}_f \mathbf{v}_b$ and/or $\nabla \mathbf{v}_b \mathbf{v}_f$ implies a low n. This is usually the case in the first few iterations of the optimization and the adaptive scheme helps in reducing the computational time by only taking a relevant number of time-steps.

7 Conclusion

In conclusion, we presented a method that lends more flexibility to the transformation model by adaptively setting the time-steps required to account for the discretization error in the numerical integration scheme. The required number of time-steps is chosen based on the properties of the velocity field prior to every optimization iteration. We showed that the Lie brackets can be conveniently represented in terms of the inverse consistency term. We showed that the proposed registration scheme solves the intra-subject registration problem equally well as the inverse consistent fixed time-step scheme by using a fewer number of time-steps.

References

1. Paul A. Yushkevich, Brian B .Avants, Sandhitsu R. Das, John Pluta, Murat Altinay, Caryne Craige, and the Alzheimer's Disease Neuroimaging Initiative. Bias in estimation of hippocampal atrophy using deformation-based morphometry arises from asymmetric global normalization: an illustration in ADNI 3T MRI data. *Neuroimage*, 50(2):434–445, April 2010.
2. G. E. Christensen and H. J. Johnson. Consistent image registration. *IEEE Transactions on Medical Imaging*, 20:568–582, 2001.
3. M. Lorenzi, N. Ayache, G. B. Frisoni, X. Pennec, and Adni. LCC-Demons: A robust and accurate symmetric diffeomorphic registration algorithm. *NeuroImage*, 81:470–483, 2013.
4. Wulf Rossmann. *Lie Groups – An Introduction Through Linear Groups*. Oxford Science Publications, 2002.
5. Akshay Pai, Stefan Sommer, Lauge Sørensen, Sune Darkner, Jon Sporring, and Mads Nielsen. Stepwise inverse consistent euler's scheme for diffeomorphic image registration. *In proceeding of workshop on Biomedical Image Registration*, pages 223–230, 2014.
6. Sai Kit Yeung and Pengcheng Shi. Stochastic inverse consistency in medical image registration. *MICCAI*, 3750:188–196, 2005.
7. A Leow, SC Huang, A Geng, J Becker, S Davis, A Toga, and P Thompson. Inverse consistent mapping in 3d deformable image registration: its construction and statistical properties. In *Information Processing in Medical Imaging*, volume 19, pages 493–503, 2005.
8. Mirza Faisal Beg and Ali Khan. Symmetric data attachment terms for large deformation image registration. *IEEE Transactions on Medical Imaging*, 26(9):1179–1189, 2007.
9. Martin Reuter, H. Diana Rosas, and Bruce Fischl. Highly accurate inverse consistent registration: A robust approach. *Neuroimage*, 53(4):1181–1196, 2010.

10. B. Avants and JC Gee. Geodesic estimation for large deformation anatomical shape averaging and interpolation. *Neuroimage*, 23(1):S139–S150, 2004.
11. Sune Darkner and Jon Sporring. Locally orderless registration. *IEEE Transactions on Pattern Analysis and Machine Intelligence*, 2012.
12. Laurent Younes. *Shapes and Diffeomorphisms*, volume 171. Springer, 2010.
13. Akshay Pai, Stefan Sommer, Lauge Sørensen, Sune Darkner, Jon Sporring, and Mads Nielsen. Image registration using stationary velocity fields parameterized by norm-minimizing wendland kernel. In *SPIE Medical Imaging*, 2015, (In press).
14. Holger Wendland. Piecewise polynomial, positive definite and compactly supported radial functions of minimal degree. *Advances in Computational Mathematics*, 4(1):389–396, 1995.
15. S Sommer, F Lauze, M Nielsen, and X Pennec. Sparse multi-scale dieomorphic registration: the kernel bundle framework. *J. of Mathematical Imaging and Vision*, 46(3):292–308, 2012.